

CHANGE DETECTION USING HIGH RESOLUTION TERRASAR-X DATA PRELIMINARY RESULTS

B. Scheuchl*, T. Ullmann, F. Koudogbo

Infoterra GmbH, Claude - Dornier-Strasse, 88039 Friedrichshafen, Germany - Bernd.Scheuchl@infoterra-global.com

KEY WORDS: Change Detection, CCD, ACD, TerraSAR-X

ABSTRACT:

This paper presents preliminary results of change detection studies using TerraSAR-X spaceborne data. Change detection is important for a variety of applications like updating maps (several years following the creation of the base map), emergency assessment following a natural catastrophe, and site monitoring. The first two cases often rely on existing geospatial information (i.e. maps) in the area of interest and involves data from different sources. Site monitoring on the other hand includes the observation of ongoing changes. Time series using an active sensor with a short revisit rate are optimal for this task. The high-resolution of TerraSAR-X and its short repeat cycle of eleven days allow reliable time series acquisitions. ACD (Amplitude Change Detection), an incoherent method, compares the backscatter of two images acquired using the same imaging parameters. It is sensitive to significant changes, i.e. changes that strongly influence the backscatter of an area. CCD (Coherence Change Detection) exploits the coherence of two SAR images acquired at different times using the same imaging parameters. They can be used to detect subtle changes occurring between the two observation dates that would remain undetected by incoherent change detection techniques. While CCD is more sensitive compared to ACD, its applicability is limited by vegetation cover. The combined use of ACD and CCD offers a more complete picture of any changes observed.

KURZFASSUNG:

Erste Ergebnisse zu Änderungsanalysen mit TerraSAR-X Satelliten werden vorgestellt. Änderungsanalysen sind für eine Vielzahl von Anwendungen geeignet, von der Aktualisierung von Karten über Informationsbereitstellung nach Naturkatastrophen oder zur Gebietsüberwachung. In den ersten beiden Fällen wird oftmals auf bestehende geographische Informationen (z.B. Karten) des Untersuchungsgebietes zurückgegriffen. Im Falle der Gebietsüberwachung werden Änderungen über einen bestimmten Zeitraum kartiert. Zur Erstellung dieser Zeitserien ist ein aktiver Sensor mit kurzer Wiederholrate und einer hohen räumlicher Auflösung sehr gut geeignet. TerraSAR-X hat eine Wiederholrate von elf Tagen und eignet sich damit gut zur Aufnahme von Zeitserien. Bei der nicht kohärenten ACD Methode (Amplituden Änderungsanalyse) werden die Rückstreuwerte von zwei Datensätzen, die mit denselben Parametern aufgenommen werden, verglichen. Im Falle der CCD Methode (Kohärenz Änderungsanalyse) wird die interferometrische Kohärenz zweier SAR-Datensätze, die mit denselben Parametern aufgenommen wurden, analysiert. Durch diese Technik können auch geringfügige Änderungen, die im Zeitraum zwischen den beiden Aufnahmen stattgefunden haben erkannt werden. Die Kohärenzanalyse kann zum Beispiel Aufschluss über die Nutzung von Pisten geben. Die höhere Sensitivität der CCD Methode im Vergleich zur ACD Methode wird in ihrer Anwendbarkeit durch das Vorhandensein von Vegetationsbedeckung eingeschränkt.

1. INTRODUCTION

Monitoring change between two dates is of interest for a number of remote sensing applications like disaster response, site monitoring and map updates. Depending on the application, requirements on the sensitivity of the measurement can vary greatly. For long term changes, the data sources may not even be identical. The challenge there is to identify changes on the required scale (i.e. finding map features that have changed between the two reference dates). Change detection is then realized on feature level. If data from the same sensor are available, the task is simplified as the two scenes can be directly compared. Change detection is carried out on the data level. Active systems provide the additional advantage of consistency of the signal provided the data are calibrated. Synthetic Aperture Radar (SAR) provides a reliable source of information for monitoring purposes and has shown to be useful for change detection (Preiss, M. et al. 2006, Wright, P. et al. 2005).

Two types of change detection may be distinguished for SAR data (pre- and post event detected SAR data acquired with the same geometry are available):

- Amplitude Change Detection - ACD
- Coherent Change Detection - CCD

This paper discusses the potential of TerraSAR-X for change detection with focus on coherent change detection. Some theoretical background is provided in Section 2. Details of data available for a test site in Utah are provided in Section 3. Results for CCD and ACD are shown in Section 4. and conclusions are drawn in Section 5.

2. BACKGROUND

2.1 TerraSAR-X

TerraSAR-X is the first radar satellite built in a Public Private Partnership (PPP) in Germany: The German Aerospace Centre

* Corresponding author.

Acquisition modes	Parameters		
	SW	POL	GRR
ScanSAR (SC)	100 km	HH or VV	1.70 -3.49 m
StripMap (SM)	30 km (sp.) 15 km (dp.)	HH or VV (sp.) HH/VV, HH/HV, VV/HV (dp.)	1.70 -3.49 m
SpotLight (SL)	10 km	HH or VV (sp.) HH/VV (dp.)	1.48 -3.49 m
High Resolution SpotLight (HS)	5–10 km	HH or VV (sp.) HH/VV (dp.)	0.74- 1.77 m (@ 300 MHz)

Table 1. TerraSAR-X acquisition modes; Abbreviations: SW: swath width, POL:Polarizations, GRR: Ground range resolution, sp.:single pol., dp.: dual pol.; (TerraSAR-X Ground Segment, 2009)

Identifier	Projection, data representation
Basic Image Products	
SSC	Single Look Slant Range, Complex representation
MGD	Multi Look Ground Range, Detected representation
GEC	Geocoded Ellipsoid Corrected, Detected representation
EEC	Enhanced Ellipsoid Corrected, Detected representation
Enhanced Image Products	
RAN ^{SAR}	Radiometrically Corrected Images
ORI ^{SAR}	Orthorectified Images
other	ADM ^{SAR} , MC ^{SAR}

Table 2. TerraSAR-X processing levels; (TerraSAR-X Ground Segment, 2009; Infoterra GmbH, 2008)

(DLR) and Astrium GmbH, a satellite system specialist, jointly developed and financed this mission. Scientific use, mission planning and operation of the satellite is the responsibility of DLR. The exploitation of TerraSAR-X data and services is conducted by Infoterra GmbH, an Astrium subsidiary, exclusively. TerraSAR-X was launched on June 15, 2007. Following a 6 month calibration phase, the sensor went operational in January 2008. Since then data are being acquired for numerous science missions and commercial customers.

Table 1 illustrates possible acquisition modes for TerraSAR-X. Available processing levels are given in Table 2.

2.2 Amplitude Change Detection

Several authors have shown that the TerraSAR-X location error of slant range products is less than one meter (TerraSAR-X Ground Segment, 2009, Schubert et al., 2008). As a result, the pixel location error of orthorectified scenes (EEC, ORI) solely depends on the quality of the underlying DEM. Consequently, orthorectified repeat pass imagery acquired using the same acquisition geometry and orbit fits pixel accurate with no additional registration step required. The resulting EEC products can therefore directly be used for ACD. GEC products can also be used for ACD with some limitations. The resulting product is not orthorectified (it is only ellipsoid corrected) which is an issue in the case of mountainous terrain, as DEM information is not considered in the processing. For flat terrain an average scene elevation included in the

processing of the GEC product will lead to a linear shift which leads to a positional error that needs to be corrected.

2.3 Coherence and Coherence Change Detection

If the complex information is to be analyzed, a coherent method can be applied for change analysis. Interferometric SAR analysis involves the formation of a complex interferogram. The resulting phase information is sensitive to terrain elevation and ground motion. In addition to the phase information, the complex interferogram contains information about the correlation of the two SAR scenes. The correlation coefficient for two zero- mean complex signals, s_1, s_2 is defined for (wide sense) stationary processes as the channel correlation for zero time shift (Touzi et. al., 1999):

$$\gamma = \frac{E \{ s_1 \cdot s_2^* \}}{\sqrt{E \{ |s_1|^2 \} \cdot E \{ |s_2|^2 \}}} \quad (1)$$

Where $E\{\}$ is the expectation value and $s_{1,2}$ are the backscattered signals. s^* describes the complex conjugate of s . While the phase of γ corresponds to the effective phase difference the magnitude of γ describes the quality of the interferometric phase and ranges from zero (no correlation) to one (full correlation). It is affected by several factors as described by (Zebker et.al., 1992a).

$$\gamma = \gamma_{temp} \cdot \gamma_{SNR} \cdot \gamma_{spec} \cdot \gamma_{vol} \quad (2)$$

γ_{temp} denotes temporal correlation. Any change of the conditions between the two data acquisitions causes decorrelation. Several reasons can be noted:

- man-made changes (e.g. agriculture, forestry)
- atmospheric effects
- changes of the dielectric properties of the backscatterer due to moisture changes
- stochastic motion (e.g. tree leaves), the effects of which can be modelled (Zebker et.al., 1992b).
- displacement. A displacement of the surface in the size of one resolution cell or more leads to complete decorrelation.

Temporal decorrelation is the dominant factor in repeat pass interferometry. Its utilization for change detection targets predominantly man-made changes.

Other factors of influence are negligible in comparison. γ_{SNR} is the decorrelation due to thermal noise. γ_{spec} is the spectral correlation, which is high for TerraSAR-X because of an orbit tube requirement limiting the baseline in combination with the sensor bandwidth. γ_{vol} describes the effect of volume backscattering .

The calculated coherence is an estimation from the data. Assuming that the processes involved are also ergodic (in mean), the sample coherence as given below can be used to estimate the coherence:

$$\hat{\gamma} = \frac{\sum_{n=1}^N s_1^{*(n)} \cdot s_2^{(n)} \cdot e^{-j\phi_T}}{\sqrt{\sum_{n=1}^N |s_1^{(n)}|^2 \cdot \sum_{n=1}^N |s_2^{(n)}|^2}} \quad (3)$$

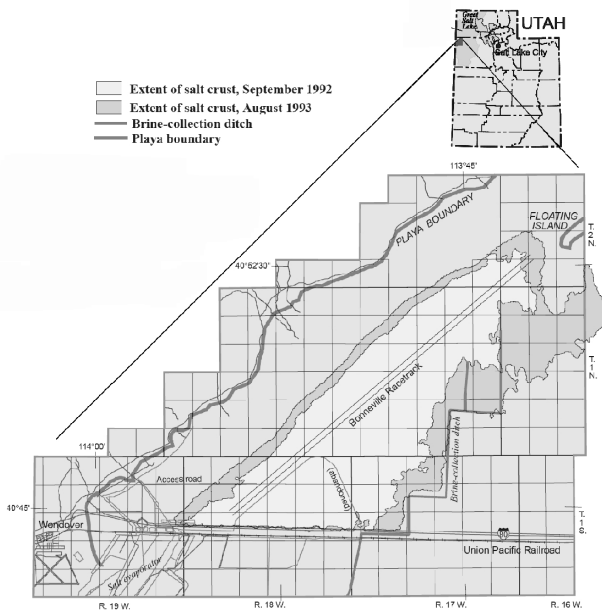


Figure 1. Sketch Map of the Bonneville Salt Flat area; (White et.al., 2003)

It is a maximum likelihood estimation where N represents the size of the estimation window. The topographic phase, ϕ_T , is compensated to remove this source of nonstationarity. This is important especially in mountainous terrain. If no topographic information is available, the local slope can be estimated by averaging the differences of adjacent phase values (tilted plane approximation) (Hagberg et.al., 1995).

3. TEST AREA – BONEVILLE SALT FLATS

3.1 Description of the test site

The test site area – Bonneville Salt Flats (BSF) - is located at the Great Salt Lake Desert – USA, about 190 km in the west of Salt Lake City. This salt flat is a playa, resulting in very low topographic energy and a plane and consistent surface structure. The test site is separated in a northern and a southern part through the Interstate 80 and the Union Pacific Railroad, which connect Wendover in a west-east direction to Reno and Salt Lake City. The BSF are flanked by the Silver Island Mountains in the north-west and a continually rising of the altitude in all other directions (White et.al., 2003). As a result of this geomorphological circumstances, the test site would be the final runoff for all surface displacements in its catchment area. Because of a very intensive surface fracturing, the precipitation runoff normally doesn't influence the surface of the playa directly. The three aquifers along the northwest end of the playa boundary are the main water transporters and collectors. To support this natural drainage system, several man-made brine-collection ditches are placed in and around the BSF (Mason et.al.,1997). The groundwater streams dissolve minerals in the underlying strata. With a general rising of the groundwater-table in winter and spring the playa is flooded every year, while the heat in summer leads to an evaporation of the brackish water, resulting in a new layer of salt coverage and a flattening of the surface. Figure 1 provides a general overview of the area.

Because of its extreme flatness, the low surface roughness and according to the annual flooding of the BSF, they are regularly

TerraSAR-X Acquisitions	Racing events
16.08.08	17.08.-24.08.08 (Race 1)
27.08.08	
07.09.08	
18.09.08	31.08.-07.09.08 (Race 2)
01.11.08	
12.11.08	17.09.-20.09.08 (Race 3)
23.11.08	
04.12.08	

Acquisition and Processing parameters	
Imaging Mode	StripMap (SM)
Polarization	HH
Incidence Angle	44.5°
Pass Direction	Descending
Processing level	SSC

Table 3. TerraSAR-X acquisitions , racing events and acquisition parameters

ROI	Description
A	Racetrack (A)
B	Racetrack (B)
C	Racetrack (C)
D	Reference – Basin D
E	Reference – Saltflat E
F	Interstate 80

Table 4. Description of regions of interest (ROI)

used for high-speed races. For such races the surface is prepared in a special way. A “Drag”, consisting of a steel I-beam structure, is towed behind a truck. So the surface is scraped and smoothed. Table 3 lists all relevant racing events taking place during the observation period.

3.2 Available Ground-truth data

To reference the results and to support the interpretation ground-truth data were obtained. Information on racing events was provided by the Utah Salt Flats Racing Association, the organizer of the relevant races. Additional datasets include weather and climate information of the weather station Wendover. They show only little precipitation events during the time of observation with an absolute maximum of 1 cm per day. One strong thunderstorm at the beginning of August 2008 with a wind speed up to 45 km/h is reported. Environmental conditions were well suited for CCD.

Digital photos of the area are also available, some even acquired around the time of TerraSAR-X data acquisition. This helped greatly in the interpretation of the analysis results.

3.3 TerraSAR-X data

A number of TerraSAR-X acquisitions, all with the same acquisition parameters, were made. Table 3 illustrates the acquisition dates and provides information on races. Figure 2 shows an averaged detected image of the area. The racing area is highlighted with a white square. The image is divided by the Interstate 80 and the Union Pacific Railroad. The southern half of the region is used for salt production. The brine drainage channels can clearly be identified as bright lines in the image.

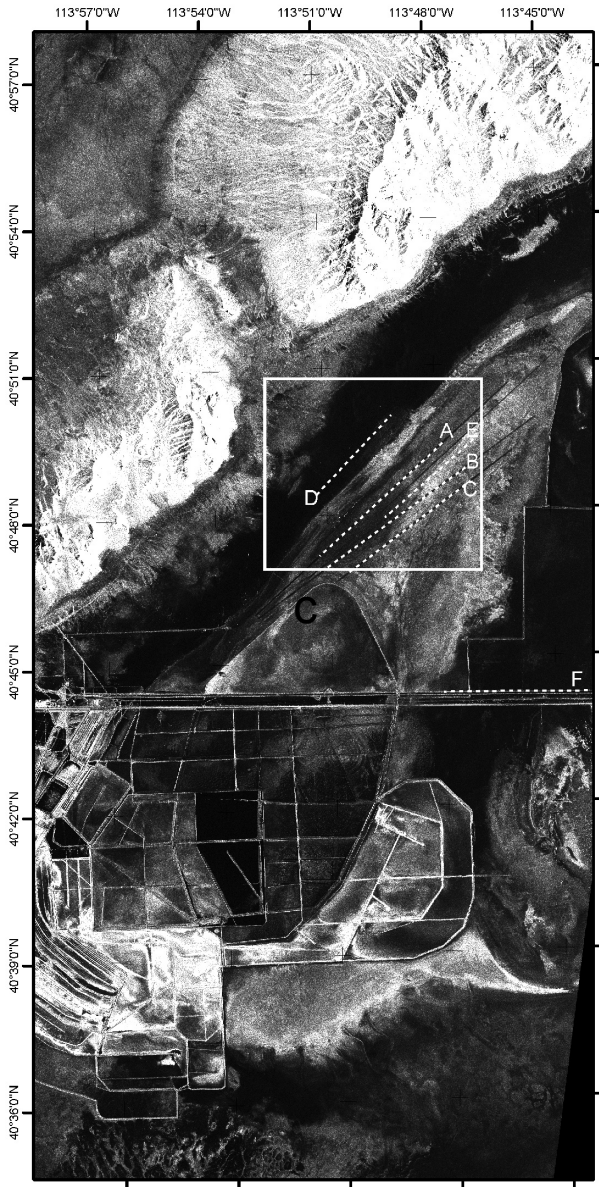


Figure 2. Averaged detected TerraSAR-X image (acquisition dates: 16.08.2008, 27.08.2008, 07.09.2008). Dashed lines (A-F indicate areas of interest for further analysis).

The dashed lines in Figure 3 indicate regions of interest (ROI), which are described in more detail in Table 4. These ROI's include racetracks, the Interstate and other areas.

4. RESULTS

4.1 CCD

For the coherence analysis the data underwent the standard interferometric processing chain, including subpixel coregistration (Massonet et.al., 1998). The interferogram was processed aiming at a ground range resolution of 6 meters. Existing DEM information (SRTM-4 DEM) was used for processing (i.e. coherence estimation and orthorectification). The coherence for each image pair was calculated using the same thresholds and moving window operators for every calculation. Results of this processing were twofold: Firstly, coherence was calculated for each eleven day interferogram.

Secondly, data pairs with more than 11 day time difference between acquisitions were also used to calculate the coherence resulting in 22-day and 33 day coherences.

With respect to the racing dates and the gap in the acquisitions from mid of August to begin of November, the second approach was aimed to identify longer term coherence. The silver island mountains, the Interstate 80, the Union Pacific railroad as well as the ditches show stable coherence. For all areas mentioned the loss of coherence over 33-days was less than 0.25. This shows the general stability of the test site – resulting from the dry surface, the low precipitation (less than 5 cm overall), and the absence of a closed vegetation cover. Reference measurements using comparable imaging parameters for areas with a high portion of vegetation approve this assumption. Loss in coherence of a 11-day cycle was at about 0.8 on open land with vegetation cover in this case. Areas without vegetation, but with dry surface, such as sand, showed comparable results to the observations made at BSF.

Figure 3 shows the results of the 11-day coherence development during the acquisition window. (Note: Min/Max values of 0 and 1 were introduced to allow better visual comparison.)

Starting with the first calculation from the acquisitions 16.08.08 and 27.08.08, the coherence clearly shows the use of the racing tracks A, B and C (see Table 3 & 4). These observations correspond to the first racing event (Race 1), which was held between the two TerraSAR-X acquisitions. Track utilization results in a lower coherence, while reference measurements and visual inspection of the ambient salt surface (E) shows a higher coherence. Reference area D shows low coherence, possibly due to flooding. Due to the use of the track the surface structure is influenced and modified, which is detectable in a change in phase of the complex SAR image. Because of the very low change in the RCS (Radar Cross Section) track utilization is particularly notable in the coherence and not in the amplitude difference. Track preparation, as described in Section 3.1, is visible in both, coherence and difference in amplitude. This results from the flattening and the compaction of the racing track, which leads to a lower surface roughness and a darker appearance in the amplitude of the SAR image. The visibility of the tracks in the coherence image therefore is the result of the intensive use and/or track preparation.

The second image in Figure 3 (27.08.08 – 07.09.08) also shows the continuous use of the racing track, which expectedly corresponds to the second racing event (Race 2). The third 11 day coherence image (07.09.08 – 19.09.08) still shows the continuous use of the racing tracks – resulting from the Race 3. Figure 3 clearly shows, that for each race different tracks and various turning points were stressed differently. The remaining coherence images (01.11.08 - 04.12.08) in Figure 3 show the strong influence of the flooding usually taking place in early winter season. Low coherence in image pair 01.11.08 – 12.11.08 indicates flooding. During this time interval there was the general raise of the groundwater table, while during the acquisitions 12.11.08 – 23.11.08 the water level begins to fall. This trend sustains also until the last acquisition (04.12.08). It shows through an increase of the coherence, resulting from the drying surface, which is more consistent in it's backscattering characteristics. Portions of some race tracks appear visible in the coherence image form pair 12.11.08 – 23.11.08. The explanation for this occurrence is that due to the preparation of the track (compacting and flattening) the drain of the water following the flooding of the area is blocked and water is kept in the traffic lane. In situ photos available confirm this assumption.

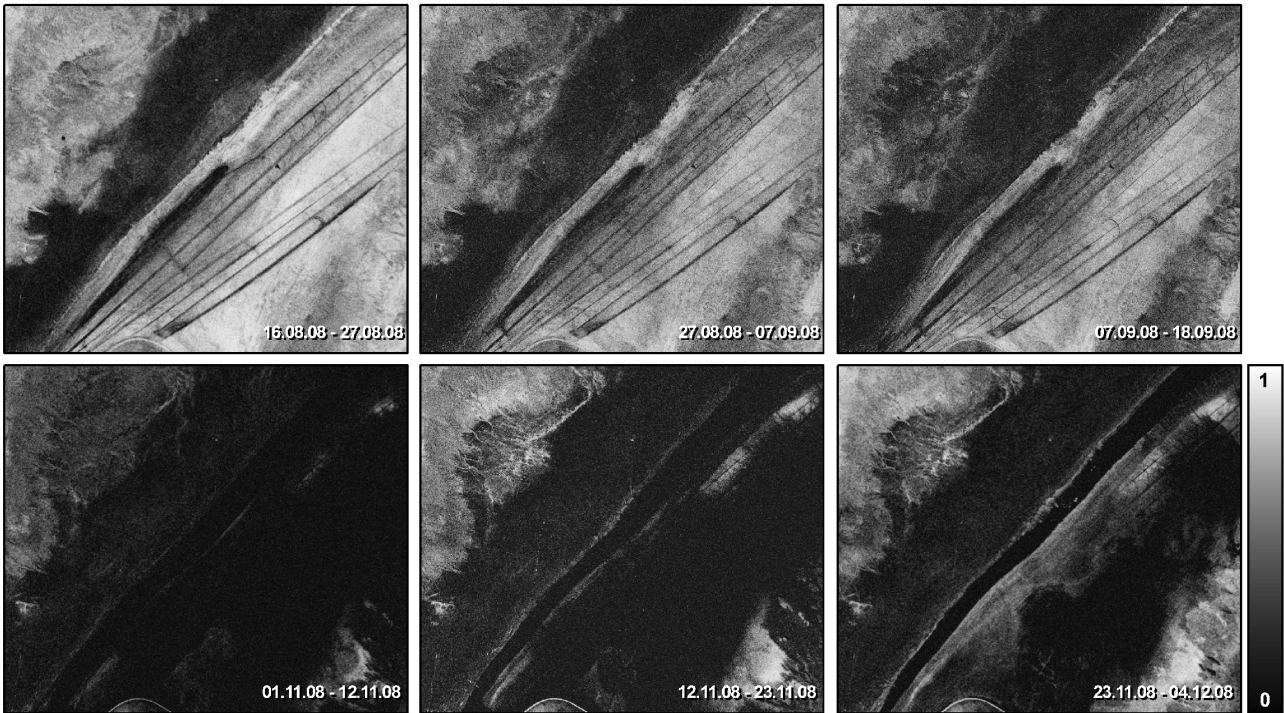


Figure 3. Calculated Coherence TerraSAR-X images.

Figure 4 shows coherence plot comparisons for the ROI's identified in Figure 2 and Table 4 for the interferometric pairs where races took place. The racetracks (A,B,C; Figure 4) show comparable coherence values. The averages range between 0.35 and 0.45. The standard deviation lies at approximately ± 0.1 . Even the min/max distribution is comparable. In difference, the reference salt flat area E (Figure 4) has a slightly higher average coherence and a significantly higher standard deviation. A pixel by pixel analysis of an area will not be successful in determining tracks and track utilization, spatial and context information is key. Reference area D has a generally low coherence. The interstate 80 (F) shows consistently high coherence. The latter has two implications. Firstly, coherence change detection cannot be used to identify the utilization of paved roads. Secondly, paved roads show relatively high coherence, a fact that can be utilized for road infrastructure identification in areas with vegetation.

4.2 ACD

In addition to coherence change detection differences in backscatter were investigated for the test site, using the same images as listed in Table 2. The results were compared to those from CCD to identify advantages and disadvantages of each method.

The the data were georeferenced, scaled to ground range resolution (multi looked), and calibrated to BetaNought. Extract results are shown in Figure 5, a and b. As additional layer the difference of the calibrated datasets was calculated (Figure 5 c). Figure 5 d shows the 11-day coherence.

As discussed in section 4.1 the amplitude of the SAR data is well suited to point out the general location of the tracks due to the change in surface roughness (compaction and flattening). This can be verified in Figure 5 c It can be seen, that an area north of racing track A was prepared between the two acquisitions. The southernmost track was widened. The turning tracks for the race cars cannot easily be identified in

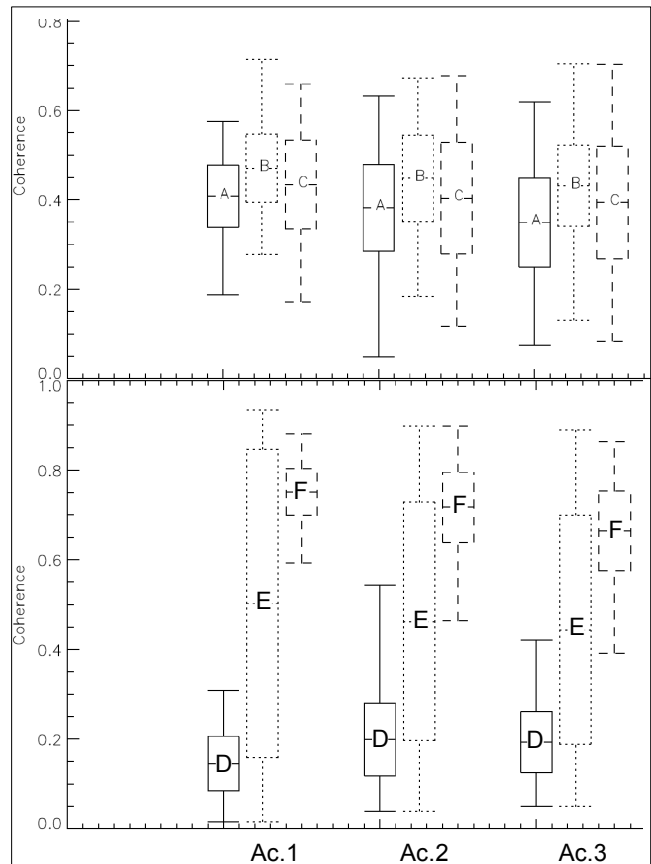


Figure 4. Coherence plot comparisons for the ROI's. (Ac.1: 16.08.-27.08.; Ac.2: 27.08.-07.09; Ac.3: 07.09.-18.09.); ROIs :A-F; recatngle: one-sigma; Span: data-range; position of letters: mean

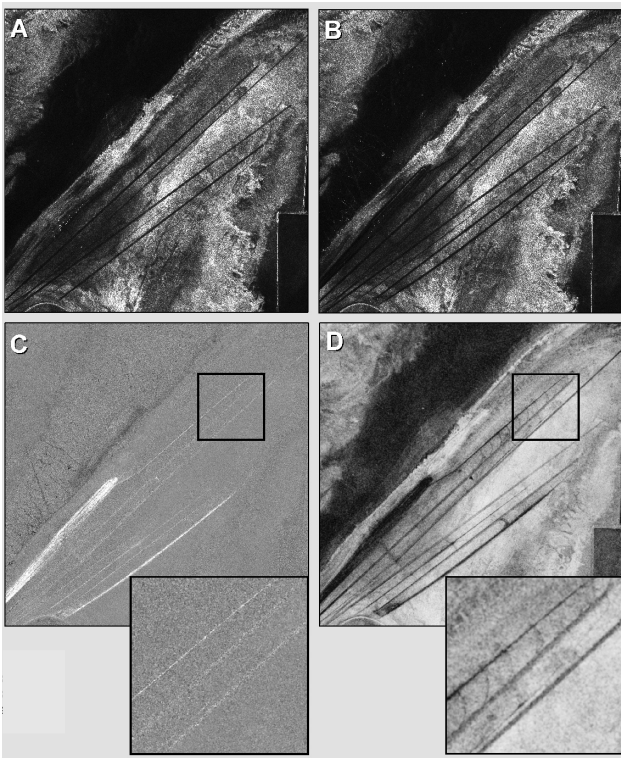


Figure 5. TerraSAR-X amplitude images (A,B), amplitude difference image (C) and coherence (D).

same geometry and the product type was chosen carefully. ACD can be applied as a side product of CCD, in this case sub-pixel accurate image registration is applied during interferometric processing. The combined use of ACD and CCD offers a more complete picture of any changes observed. Future steps include an investigation on the geographic transferability of the method as well as and analysis of potential applications. While some limitations were identified, a broader set of recommendations on the applicability of the methods is required.

5. CONCLUSIONS

The use of coherence change detection clearly shows that track utilization can be observed over dry, non vegetated areas. Ancillary information for the area of interest (e.g. environmental conditions) will aid the interpretation of the result. Context information and spatial analysis are important for the identification of changes due to human activities on tracks. A general limitation is the presence of vegetation which leads to decorrelation even for 11 day interferograms. The utilization of paved roads cannot be determined, however, there is clear indication that X-band coherence shows potential for road infrastructure detection in areas with vegetation cover. TerraSAR-X orbit requirements are particularly suited for interferometric applications. Amplitude change detection is less sensitive to subtle changes, but it is much more robust and still provides valuable information. The high positional accuracy of TerraSAR-X allows the application of ACD without the need of additional image co-registration, provided pre- and post event detected SAR data were acquired with the same geometry and the product type was chosen carefully. ACD can be applied as a side product of CCD, in this case sub-pixel accurate image registration is applied during interferometric processing. The combined use of ACD and CCD offers a more complete picture of any changes observed. Future steps include an investigation on the geographic

transferability of the method as well as and analysis of potential applications. While some limitations were identified, a broader set of recommendations on the applicability of the methods is required.

ACKNOWLEDGEMENTS

The authors would like to thank Mr. Wester Potter, Dan Wright and their team from the Media Relations, Utha Salt Flats Racing Association for the provided information.

REFERENCES

- Infoterra GmbH, 2008. TerraSAR-X Radar Image Portfolio, Friedrichshafen Germany. <http://www.infoterra.de/terrasar-x/radar-imagery.html> (accessed 20. Apr. 2009)
- Hagberg, J. O., Ulander, L. M. H., and Askne, J. 1995. Repeat-pass SAR interferometry over forested terrain, *IEEE Transactions on Geoscience and Remote Sensing*, vol. 33, no. 2, pp.331-340
- Mason, J. L. and Kipp, Jr., K. L. 1997. Investigation of Salt Loss from the Bonneville Salt Flats, Northwestern Utah. *U.S. Department of the Interior—U.S. Geological Survey, USGS Online Publications – FS97-135*
- Massonet, D. and Feigl, K. L. 1998. Radar Interferometry and its Application to Changes in the Earth's Surface, *Reviews of Geophysics*, vol. 36, no. 4, pp. 441-500
- Preiss, M. and Stacy, N.J.S. 2006. Coherent Change Detection: Theoretical Description and Experimental Results, DSTO-TR-1851
- TerraSAR-X Ground Segment. 2009. *Basic Product Specification Document*. TX-GS-DD-3302, Issue 1.6
- Schubert, A; Jehle, M; Small, D; Meier, E. 2008. Geometric validation of TerraSAR-X high-resolution products. *In: 3rd TerraSAR-X Science Team Meeting, Oberpfaffenhofen, DE, 25. 26. November 2008*
- Touzi, R., Lopez, A., Bruniquel, J. and Vachon, P. W. 1999. Coherence Estimation for SAR Imagery, *IEEE Transactions on Geoscience and Remote Sensing*, vol. 37, no. 1, pp. 135-149
- White, W.W. III, P.G. 2003. Replenishment of Salt to the Bonneville Salt Flats: Results of the 5-Year Experimental Salt Laydown Project. *Betting on Industrial Minerals, Proceedings of the 39th Forum on the Geology of Industrial Minerals, Sparks, 2003: Nevada Bureau of Mines and Geology Special Publication 33, Nevada, May 19–21*
- Wilberg, D.E. Tibbetts, J.R., Enright, M., Burden, C.B., Smith, C., and Angerth, C.E. 2005. *Water Resources Data Utah Water Year 2005 - Water-Data Report UT-05-1*. U.S. Geological Survey
- Wright, P. Macklin, T., Willis, C., Rye, T. 2005. Coherent Change Detection with SAR. *2nd EMRS DTC Technical Conference, Edinburgh*
- Zebker, H. A. and Villasenor, J. 1992a. Decorrelation in interferometric radar echoes, *IEEE Transactions on Geoscience and Remote Sensing*, vol. 30, no. 5, pp. 950-959
- Zebker, H. A. and Villasenor, J. 1992b. Studies of temporal change using radar interferometry, *SPIE Synthetic Aperture Radar*, vol. 1630, pp.187-198